ISSN: 2414-1895 DOI: 10.6919/ICJE.202105_7(5).0039

Control and Modeling of Modular Multi-level High Voltage Converter Vector for Rail Trail Traction

Xun Wang#, Liujian Zhang#, Pingbo Wu*

State Key Laboratory of Traction Power, Southwest Jiaotong University, Chengdu, Sichuan, China.

*731182320@qq.com

#These authors contributed equally to this work.

Abstract

The modular multilevel converter has the advantages of small harmonic, good power quality output waveform, high reliability and no need of input filtering and power compensation, so it is suitable for the field of frequency conversion. The traction transmission system realizes the speed regulation of the rail vehicle, which is very important for the rail vehicle system. The traction drive system adjusts the running speed and traction force of the train by controlling the frequency and amplitude of the input voltage of the traction motor. In this paper, the modular multi-level high voltage vector control is used to find that the input voltage and current harmonic content of motor is low, the efficiency is high, the output voltage is close to sine wave, and the structure is simple and easy to realize with well motor performance.

Keywords

Traction Transmission System; Rail Vehicle; High Voltage Converter Vector.

1. Introduction

AC speed regulation technology can improve the automation level, improve the process, and improve the product quality and labor productivity, and improve the production environment. The technology of frequency conversion has excellent speed regulation and braking performance, high efficiency, high power factor and good energy saving effect, which makes it have a good development prospect. The frequency converter can meet the requirements of motor speed control in rail transit, while improving the speed of rail transit vehicles, saving energy and reducing production cost. At present, the motor can save about 30% of the electric energy on average if the frequency converter is used. Therefore, the input and use of the inverter is a good energy saving measure. The traction drive system [1-6] for rail vehicles mainly includes traction converter, traction motor and gear drive system. The traction inverter [7-9] controls the power semiconductor element(IGBT) through the gate drive unit, converts the intermediate DC into three-phase AC to supply the asynchronous traction motor, controls the motor rotation, and then drives the whole train forward.

Modular multi-level high voltage inverter [10] has low harmonic pollution to the power grid, good power quality output waveform, high reliability, no need of input filtering and power compensation, and no torque ripple, common mode voltage and other problems caused by harmonics, so it is also called perfect harmonic free inverter, which is suitable for ordinary asynchronous motor. Modular multi-level high-voltage converter uses several low-voltage power units in series to achieve high-voltage output. Compared with two-level and three-level converters, it has more output levels and better sinusoidal output waveform. In order to reduce the input current harmonics, the phase-shifting input transformer of frequency converter adopts multiple structures. The high voltage frequency

ISSN: 2414-1895 DOI: 10.6919/ICJE.202105_7(5).0039

conversion system has 15 power units, which are powered by 15 secondary windings of the phase-shifting input transformer, and each of the three windings is a phase group, and each phase group is 12° different from each other. In theory, the input current waveform is close to sine wave, and the total current harmonic distortion rate is less than 1%.

According to the principle of motor [4,9,11-18] converts the electric energy of the catenary into mechanical energy through energy conversion, the key of motor control is the control of electromagnetic torque. The reason why DC motor has good control performance is that its torque is easy to control. The situation of asynchronous motor is complex. The torque of induction motor is not only related to air gap flux and rotor current, but also depends on the power factor of rotor current. The complexity of its torque makes it difficult to control induction motor. Vector control is a high performance control method of induction motor. The idea is that the stator current is decoupled into excitation component and torque component by coordinate transformation. These two components are independent of each other. The purpose of controlling the magnetic field and torque can be achieved by controlling them separately, which makes the asynchronous motor control have the same excellent performance as the DC motor control.

2. Establishment of modular multi-level high voltage inverter model

2.1 Circuit model of modular multi-level high voltage inverter

Each phase of the modular multi-level high voltage inverter is composed of five identical power units in series, and the three phases are Y-type connection, which directly outputs the high voltage of variable frequency and variable voltage required by the motor. The main components of modular multi-level high-voltage converter are phase-shifting input transformer, main circuit of inverter and high voltage motor, as shown in Fig. 1.

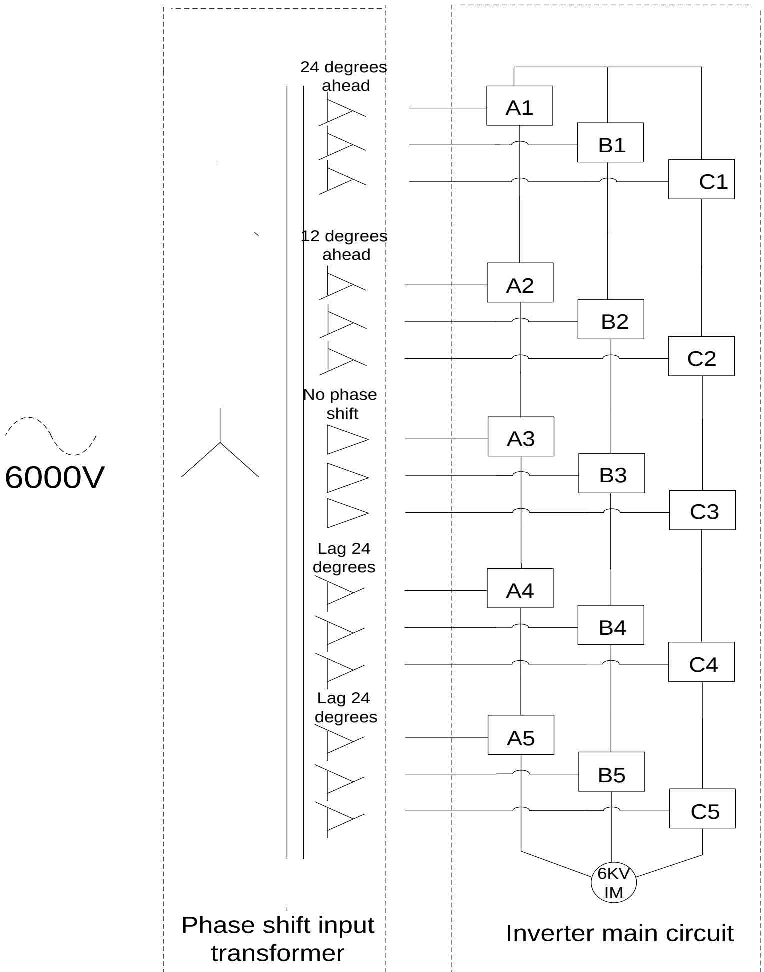

Fig. 1 Structure diagram of modular multi-level high-voltage inverter.

ISSN: 2414-1895 DOI: 10.6919/ICJE.202105_7(5).0039

Assuming that the number of power units in series in each phase is N, the number of output phase voltage levels is as follows:

$$M = 2N + 1 \tag{1}$$

H-bridge switching function is as follows:

$$H_k = \begin{cases} 1 & S_1 \\ 0 & S_2 / S_3 \, (k = 1, 2, 3 \ldots N) \\ -1 & S_4 \end{cases} \tag{2}$$

Where H is the switch state, the definition is shown in table 1, where (k = 1, 2, 3, …, N)

Table 1. Switch status of modular multi-level high-voltage inverter.

	V_{k1}	V_{k2}	V_{k3}	V_{k4}
S_1	On	Off	Off	On
S_2	On	Off	On	Off
S_3	Off	On	Off	On
S_4	Off	On	On	Off

When the DC bus voltage of H-bridge unit is V_0, the single-phase output voltage is as follows:

$$V_{XN} = \sum_{k=1}^{N} H_k \times V_0 (X : A/B/C) \tag{3}$$

The circuit structure of the power unit is shown in Fig. 2. Its working principle is as follows: after the three-phase AC is rectified by the diode uncontrolled full bridge rectifier circuit, the DC bus voltage is formed by the filter capacitor. The output side is the H-bridge single-phase inverter circuit composed of four IGBT modules, and the output voltage of variable voltage and frequency conversion is obtained by PWM modulation. Because the rectifier part of power unit is diode without control rectifier structure, it cannot achieve energy feedback, so it cannot operate in four quadrants. The filter capacitor provides the required reactive power for the motor, so the input power factor of the power unit can reach above 0.95 without power factor compensation.

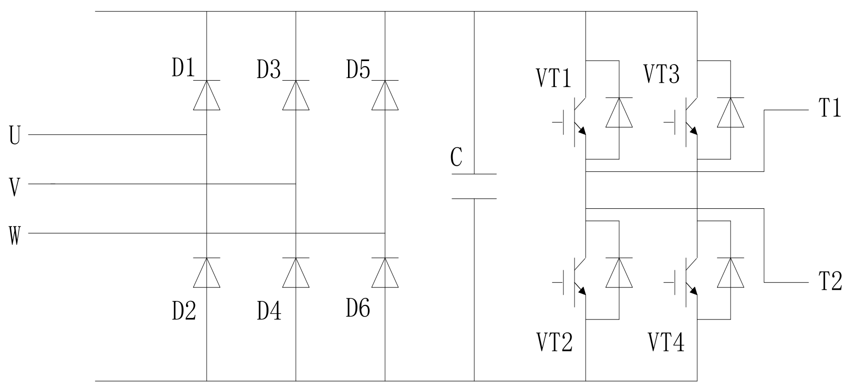

Fig. 2 Structure diagram of circuit for the power unit [10].

2.2 Modulation algorithm of modular multi-level high voltage inverter

When five power units are connected in series, SPWM modulation is completed by five triangular carriers and a pair of inverted sinusoidal modulated wave signals. The shape of the five triangular carriers is the same, but the phase angle is $T_s/5$ in turn, T_s is the carrier period. The phase of the left arm modulation wave is the same as that of the output voltage, but the phase of the right arm modulation wave is the opposite, as shown in Fig. 3.

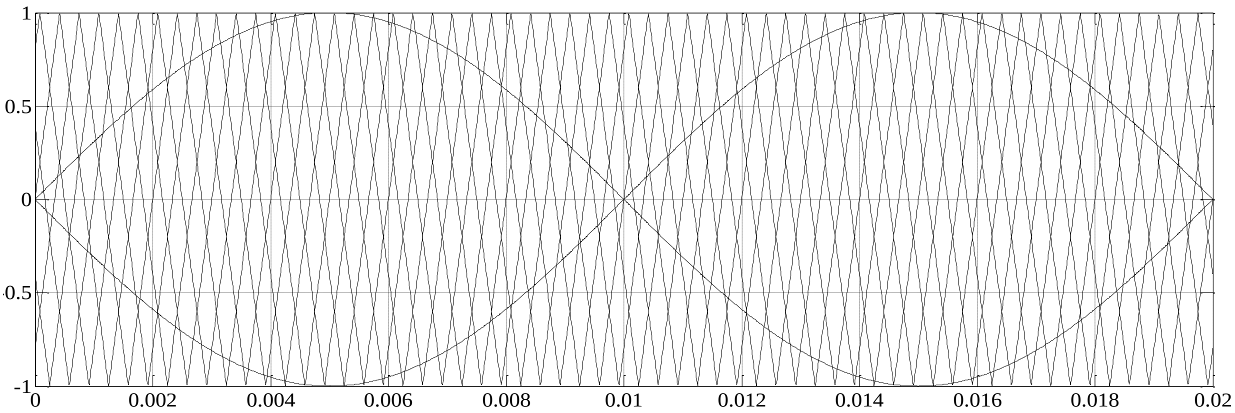

Fig. 3 Schematic diagram of the working principle for phase modulation.

By Fourier decomposition of the output voltage of the left leg of A-phase single power unit, the output voltage relationship of the left leg of the power unit can be obtained

$$U_{a11} = \frac{ME}{2}\cos(\omega t) + \frac{2E}{\pi}\sum_{m=1}^{\infty}\sum_{n=-\infty}^{\infty}\frac{1}{m}\left\{\sin[(m+n)\frac{\pi}{2}]J_{\mathrm{n}}(m\frac{\pi}{2}M)\cos(m\omega_{\mathrm{c}}t + n\omega t)\right\} \tag{4}$$

Where: E—DC bus voltage of power unit, M—Modulation ratio, ω—frequency of output fundamental voltage, ω_c —frequency of triangular carrier.

Because the phase difference between the left and right arms of the same power unit is 180°, the expression of the output voltage of a single power unit in phase A is as follows:

$$U_{\mathrm{a1}} = U_{\mathrm{a11}} - U_{\mathrm{a12}} = ME\cos(\omega t) + \frac{4E}{\pi}\sum_{m=1}^{\infty}\sum_{n=-\infty}^{\infty}\frac{1}{m}\cdot\{\cos[(m+n+1)\pi]J_{\mathrm{2n\text{-}1}}m\pi M \cdot\cos[2m\omega_{\mathrm{c}}t + (2n-1)\omega t]\} \tag{5}$$

When N power units are in series, the expression of output phase voltage is:

$$U_{\mathrm{a}} = \sum_{i=1}^{N}U_{\mathrm{ai}} = NME\cos(\omega t) + \frac{4E}{\pi}\sum_{m=1}^{\infty}\sum_{n=-\infty}^{\infty}\frac{1}{m}\cdot\{\cos[(m+n+1)\pi]J_{\mathrm{2n\text{-}1}}m\pi M \cdot\sum_{i=1}^{N}\cos[2m(\omega_{\mathrm{c}}t + \frac{i\pi-\pi}{N}) + (2n-1)\omega t]\} \tag{6}$$

For a single power unit, the output voltage harmonic is concentrated near the frequency of 2 times of carrier, while when the five power units are in series, the output voltage harmonic is concentrated near the carrier frequency of 10 times. So even if the triangular carrier frequency of each power unit is not high, the whole system has a higher equivalent carrier frequency, which can reduce the loss of power switch tube.

The two modulated waves of the power unit are provided by the two phases respectively. Different from the in-phase modulation, the modulation wave of the left and right arms of the power unit changes: the phase of the modulation wave of the left arm is the same as that of the output voltage, while the phase angle of the modulation wave of the right arm lags 120 degrees, as ahown in Fig. 4. Taking the modulation wave of left and right bridge arms of phase a power unit as an example, the expression is as follows:

$$\begin{cases} f_{a1} = M\sin(\omega t) \\ f_{a2} = M\sin(\omega t - 2\pi/3) \end{cases} \tag{7}$$

ISSN: 2414-1895 DOI: 10.6919/ICJE.202105_7(5).0039

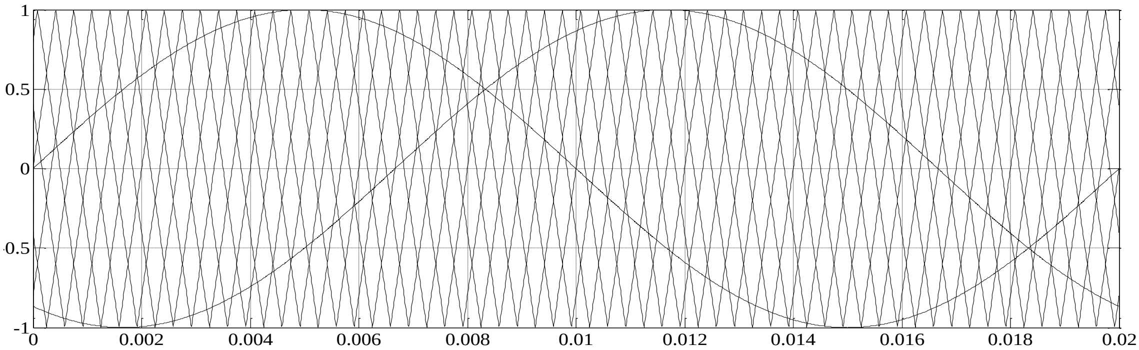

Fig. 4 Schematic diagram of out-phase modulation principle.

Then the output voltage of single power unit and phase a meets the following requirements:

$$\begin{cases} U_{a1} = \dfrac{\sqrt{3}}{2} ME \sin(\omega t + \pi/6) \\ U_{\mathrm{AN}} = \sum_{n=1}^{5} U_{\mathrm{an}} ME \sin(\omega t + \pi/6) \end{cases} \tag{8}$$

2.3 Realization of vector control method

In the two phase arbitrary rotating coordinate system (*dq* coordinate system), the mathematical model of asynchronous motor can be expressed as the following matrix equation:

Torque equation

$$T_{\mathrm{e}} = n_{\mathrm{p}} L_{\mathrm{m}} (i_{\mathrm{sq}} i_{\mathrm{rd}} - i_{\mathrm{sd}} i_{\mathrm{rq}}) \tag{9}$$

Equation of motion

$$T_{\mathrm{e}} = T_{\mathrm{L}} + \frac{J}{n_{\mathrm{p}}} \frac{d_{\omega_{\mathrm{r}}}}{dt} \tag{10}$$

Where: i_{sd}—d axis component of stator current; i_{sq}—q axis component of stator current; i_{rd}—d axis component of rotor current; i_{rq}—q axis component of rotor current; L_{m}—Mutual inductance of two phase winding; n_{p}—Polar logarithm; J—Moment of inertia; ω_{r}—Angular velocity of motor rotor.

The mathematical model of vector control is established in the synchronous rotating coordinate system based on rotor field orientation. The vector control is changed into scalar control in the synchronous rotating coordinate system, and the nonlinear decoupling in the magnetic field orientation is used to improve the dynamic characteristics of the system. In the case of rotor magnetic field orientation, the basic equation of voltage in MT coordinate system is as follows:

$$\begin{bmatrix} U_{\mathrm{sM}} \\ U_{\mathrm{sT}} \\ 0 \\ 0 \end{bmatrix} = \begin{bmatrix} L_{\mathrm{s}}P + R_{\mathrm{s}} & -\omega_{\mathrm{s}} L_{\mathrm{s}} & L_{\mathrm{m}}P & -\omega_{\mathrm{s}} L_{\mathrm{m}} \\ L_{\mathrm{s}}\omega_{\mathrm{s}} & R_{\mathrm{s}} + L_{\mathrm{s}}P & \omega_{\mathrm{s}} L_{\mathrm{m}} & L_{\mathrm{m}}P \\ L_{\mathrm{m}}P & 0 & R_{\mathrm{r}} + L_{\mathrm{r}}P & 0 \\ \omega_{\mathrm{sl}} L_{\mathrm{m}} & 0 & \omega_{\mathrm{sl}} L_{\mathrm{r}} & R_{\mathrm{r}} \end{bmatrix} \begin{bmatrix} i_{\mathrm{sM}} \\ i_{\mathrm{sT}} \\ i_{\mathrm{rM}} \\ i_{\mathrm{rT}} \end{bmatrix} \tag{11}$$

The flux linkage equation is as follows

$$\begin{bmatrix} \psi_{\mathrm{sM}} \\ \psi_{\mathrm{sT}} \\ \psi_{\mathrm{rM}} \\ 0 \end{bmatrix} = \begin{bmatrix} L_{\mathrm{s}} & 0 & L_{\mathrm{m}} & 0 \\ 0 & L_{\mathrm{s}} & 0 & L_{\mathrm{m}} \\ L_{\mathrm{m}} & 0 & L_{\mathrm{r}} & 0 \\ 0 & L_{\mathrm{m}} & 0 & L_{\mathrm{r}} \end{bmatrix} \begin{bmatrix} i_{\mathrm{sM}} \\ i_{\mathrm{sT}} \\ i_{\mathrm{rM}} \\ i_{\mathrm{rT}} \end{bmatrix} \tag{12}$$

ISSN: 2414-1895 DOI: 10.6919/ICJE.202105_7(5).0039

3. Results and discussion

The main circuit of the simulation model does not consider the phase-shifting transformer, the power unit is powered by DC power supply, each phase is composed of five power units in series, and the third harmonic is injected into the input.

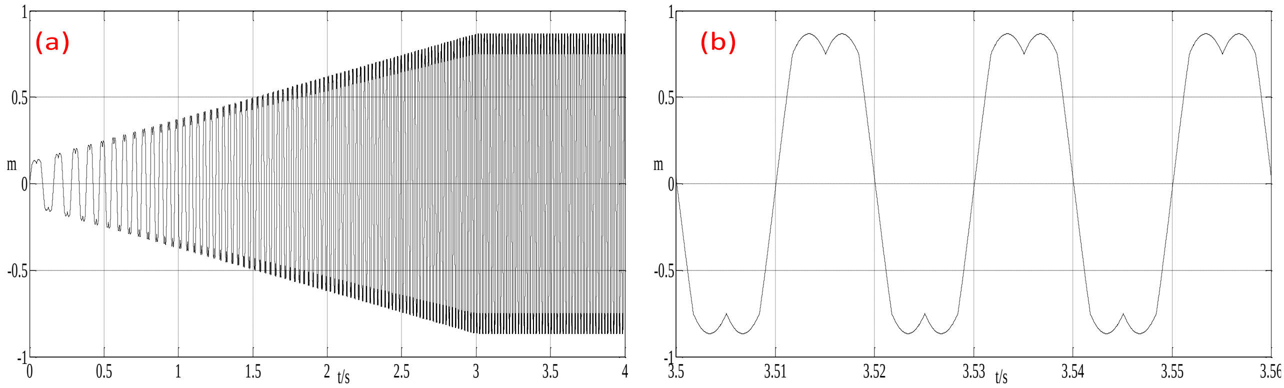

Fig. 5 Modulation wave (a), and its amplified waveform (b) for motor control model.

The modulation waveform is shown in Fig. 5, it is showed non sinusoidal state, as to waveform injected 3 harmonics. When the system starts, the amplitude increases continuously, and the amplitude remains unchanged after 3 seconds.

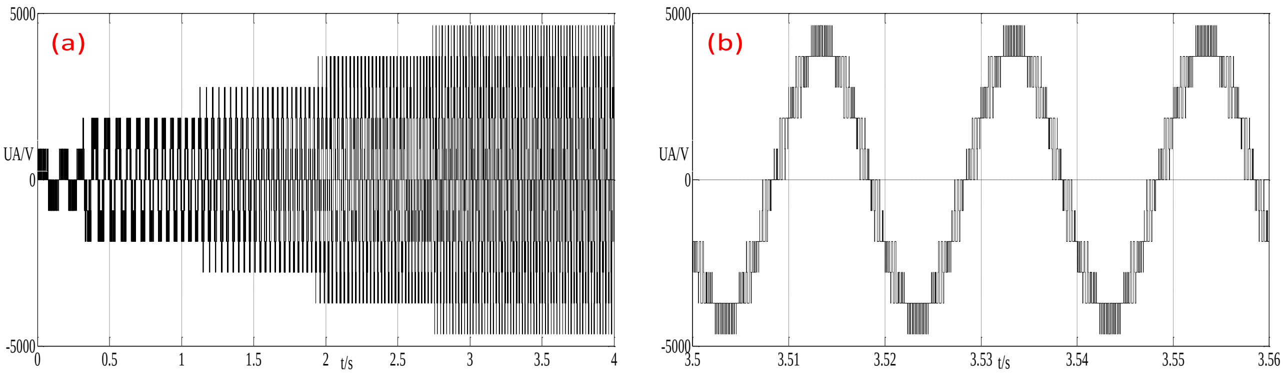

Fig. 6 Phase voltage waveform (a) and its amplified waveform (b) of inverter output for motor control model.

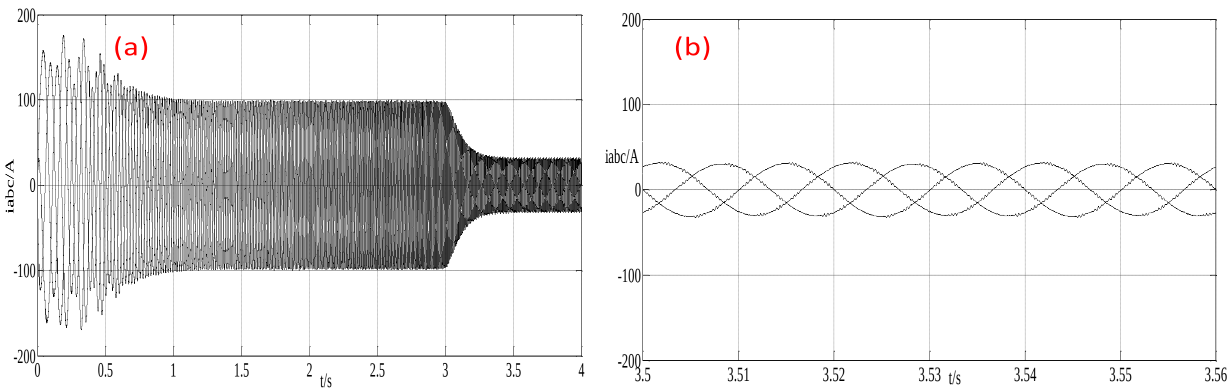

Fig. 7 Three phase stator current waveform (a) and its amplified waveform (b) for motor control model.

ISSN: 2414-1895
DOI: 10.6919/ICJE.202105_7(5).0039

As can be seen from Fig. 6, with the increase of time, the phase voltage amplitude of inverter output increases gradually, and remains unchanged after 2.75 seconds. At the same time, it can be found that the level number of output phase voltage is eleven, which satisfies the relationship of $2N + 1$ when the number of cascades is N.

The three-phase stator current gradually decreases with the increase of time, which is stable after 3.5 seconds, as shown in Fig. 7. It is found that when the system starts up, the peak current is about 100A, and the effective value is 71A, which is about 1.3 times of the rated current. The starting current is small, which can reduce the impact on the power grid. According to the enlarged three-phase current waveform, the stable current waveform is a perfect sine wave with a phase difference of 120 degrees.

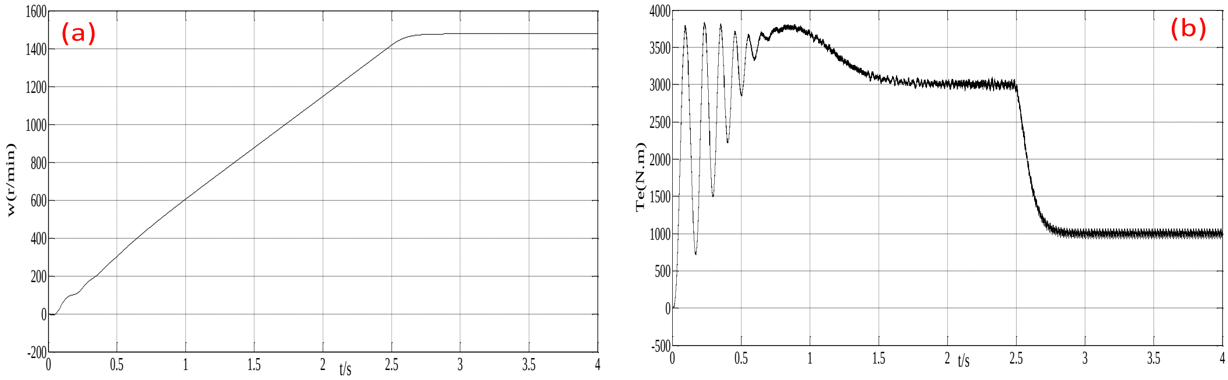

Fig. 8 Speed waveform (a) and torque waveform (b) for motor control model.

It can be seen from the speed waveform that the motor speed increases gradually after the system starts, and the motor starts after 2.5 seconds, and then the motor speed basically reaches a stable speed, which is about 1450 r/min. It can be seen from the output torque waveform of the motor that in the process of motor speed-up, except for 0.5 seconds of starting, the motor torque fluctuates greatly, and the other time torque basically remains constant, about 3100 $N \cdot \mathrm{m}$, about 1.05 times of the rated torque. After the motor starts, the torque gradually tends to be stable, about 1000 $N \cdot \mathrm{m}$. Therefore, in the process of variable frequency starting, the motor starting torque is small, the fluctuation is small, the starting torque is stable, and the impact on the motor and its load is small.

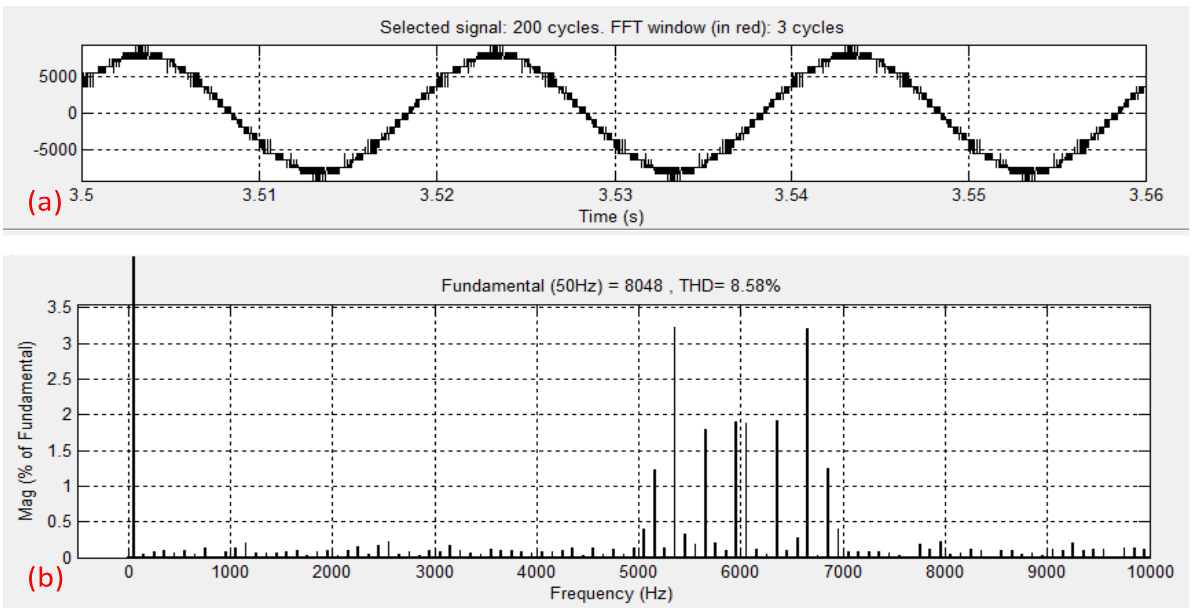

Fig. 9 Time domain diagram (a) and frequency domain diagram (b) of line voltage.

ISSN: 2414-1895 DOI: 10.6919/ICJE.202105_7(5).0039

When the inverter operates at 50 Hz, the harmonic distribution of the output line voltage is shown in Figure 9. It can be seen from the figure that the amplitude of line voltage is about 10000 V, and its low order harmonic content is very small, harmonic is mainly concentrated around 6000 Hz corresponding to the output equivalent switching frequency, ranging from 5000 Hz to 7000 Hz, the highest harmonic content is 3.25%. The THD of the output line voltage is 8.58%, which meets the power supply requirements of ordinary motors.

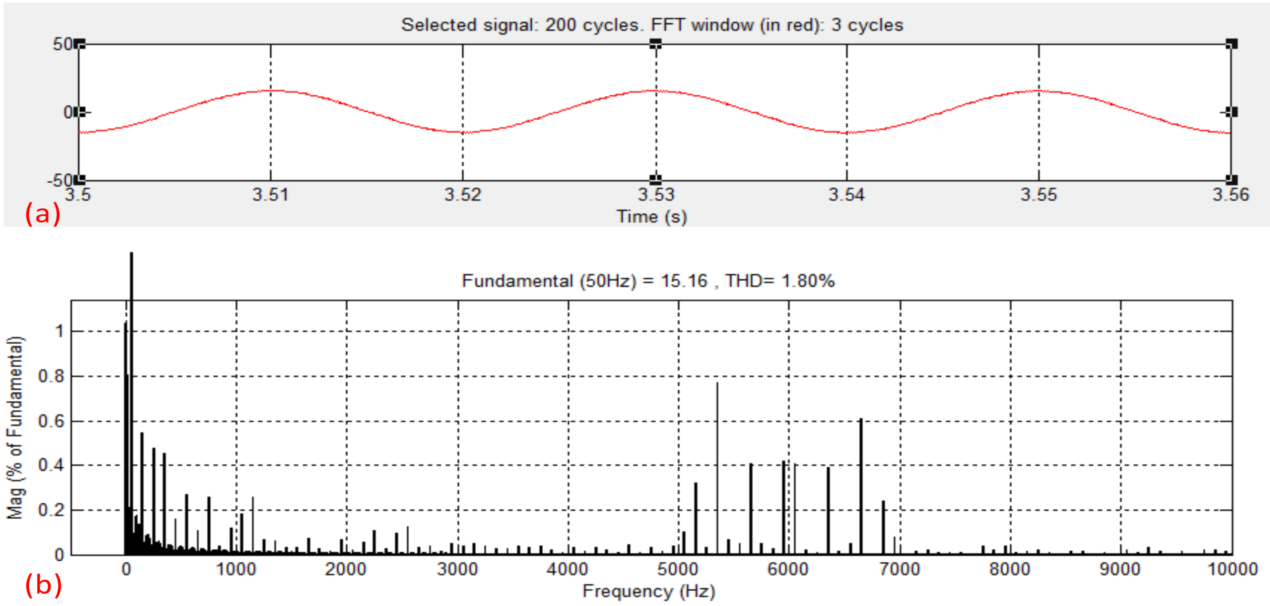

Fig. 10 Time domain diagram (a) and frequency domain diagram (b) of output current.

Fig. 10 shows the spectrum distribution of the output current when the system operates at 50 Hz. It can be seen from the figure that the current of the motor in steady state has good sinusoidal degree, and the waveform is relatively smooth. Its amplitude is about 20A, and the total current THD is only 1.80%. The current harmonics are mainly concentrated around 6000Hz corresponding to the output equivalent switching frequency and below 1000Hz, and the other harmonic current content is very small.

4. Conclusions

As one of the most important members in the area of transportations, rail train has been the core of national economic development. Compared with other transportation ways, such as highway, aviation or sea transportation, rail vehicle transportation has the advantages of long distance, low costing, high safety rate, large volume and low environmental pollution. Rail vehicle transportation plays a significant role in the social and economic life in China and all around the world, especially some high-population countries or areas. Motor control system based on modular multi-level high voltage has the advantages of less harmonic pollution on the input side, high efficiency, output voltage close to sine wave, simple structure and easy implementation.

Acknowledgments

This paper was supported by national Natural Science Foundation of China (U1934202).

References

[1] Mao, Z., et al., Adaptive Fault-Tolerant Sliding-Mode Control for High-Speed Trains With Actuator Faults and Uncertainties. Ieee Transactions on Intelligent Transportation Systems, 2020. 21(6): p. 2449-2460.

ISSN: 2414-1895 DOI: 10.6919/ICJE.202105_7(5).0039

[2] Scheepmaker, G.M. and R.M.P. Goverde, Energy-efficient train control using nonlinear bounded regenerative braking. Transportation Research Part C-Emerging Technologies, 2020. 121.

[3] Su, S., et al., An Energy-Efficient Train Operation Approach by Integrating the Metro Timetabling and Eco-Driving. Ieee Transactions on Intelligent Transportation Systems, 2020. 21(10): p. 4252-4268.

[4] Wang, J., et al., Nonsmooth Dynamics of a Gear-Wheelset System of Railway Vehicles Under Traction/Braking Conditions. Journal of Computational and Nonlinear Dynamics, 2020. 15(8).

[5] Wang, P., et al., Train trajectory optimization for improved on-time arrival under parametric uncertainty. Transportation Research Part C-Emerging Technologies, 2020. 119.

[6] Yildirim, D., et al., Full-Scale Physical Simulator of All SiC Traction Motor Drive With Onboard Supercapacitor ESS for Light-Rail Public Transportation. Ieee Transactions on Industrial Electronics, 2020. 67(8): p. 6290-6301.

[7] Hao, F., et al., Optimal Voltage Regulation and Power Sharing in Traction Power Systems With Reversible Converters. Ieee Transactions on Power Systems, 2020. 35(4): p. 2726-2735.

[8] Kersten, A., et al., Battery Loss and Stress Mitigation in a Cascaded H-Bridge Multilevel Inverter for Vehicle Traction Applications by Filter Capacitors. Ieee Transactions on Transportation Electrification, 2019. 5(3): p. 659-671.

[9] Zhong, Z., et al., Hierarchical Optimization of an On-Board Supercapacitor Energy Storage System Considering Train Electric Braking Characteristics and System Loss. Ieee Transactions on Vehicular Technology, 2020. 69(3): p. 2576-2587.

[10] Zhang, L., The Simulation Research on Sensorless Vector Control System of The Modular Multi-level High-Voltage Inverter. 2014.

[11] Liu, H., et al., Research on energy-saving characteristics of battery-powered electric-hydrostatic hydraulic hybrid rail vehicles. Energy, 2020. 205.

[12] Liu, J., et al., Wheel/Rail Adhesion State Identification of Heavy-Haul Locomotive Based on Particle Swarm Optimization and Kernel Extreme Learning Machine. Journal of Advanced Transportation, 2020. 2020.

[13] Liu, Y., et al., Dynamic investigation of traction motor bearing in a locomotive under excitation from track random geometry irregularity. International Journal of Rail Transportation, 2021.

[14] Luo, J., S. Zhu, and W. Zhai, Theoretical modelling of a vehicle-slab track coupled dynamics system considering longitudinal vibrations and interface interactions. Vehicle System Dynamics, 2020.

[15] Qi, Y. and H. Dai, Influence of motor harmonic torque on wheel wear in high-speed trains. Proceedings of the Institution of Mechanical Engineers Part F-Journal of Rail and Rapid Transit, 2020. 234(1): p. 32-42.

[16] Wang, Z., et al., Wheel wear analysis of motor and unpowered car of a high-speed train. Wear, 2020. 444.

[17] Wang, Z., et al., Coupled dynamic behaviour of a transmission system with gear eccentricities for a high-speed train. Vehicle System Dynamics, 2020.

[18] Yao, B., et al., Multitimescale Reliability Evaluation of DC-Link Capacitor Banks in Metro Traction Drive System. Ieee Transactions on Transportation Electrification, 2020. 6(1): p. 213-227.